Waterborne Polyurethane with Biobased Internal Emulsifier

Highlights

This chapter describes the utilization of glycerol ester of citric acid (GECA) as an internal emulsifier for preparing high-performance biobased anionic waterborne polyurethane (WPU) like PU dispersions (PUDs), as density functional theory (DFT) calculations reveal that it has comparable reactivity to conventional dimethyl propionic acid (DMPA). GECA was prepared by an esterification reaction between citric acid and glycerol. GECA-based WPU was obtained by reacting it with isophorone diisocyanate in the presence of poly(ε-caprolactone) diol, monoglyceride of castor oil (MG_{CO}), and other desired reactants, using a pre-polymerization process. Films obtained from this WPU exhibited high stretchability, good tensile strength, high toughness, optimal thermal stability, moderate to high transparency, and satisfactory chemical and UV resistance attributes. Most importantly, WPU films also showed profound biodegradation under the exposure of *B. subtilis* bacterial strain.

Parts of this chapter are published in

Morang, S., Biswakarma, N., Deka, R.C. and Karak, N. Citric acid/glycerol ester, a backup of 2, 2-bis (hydroxymethyl) propionic acid and biobased synthesis of anionic polyurethane dispersion. *Progress in Organic Coatings*, 168:106880, 2022. (DOI: 10.1016/j.porgcoat.2022.106880)

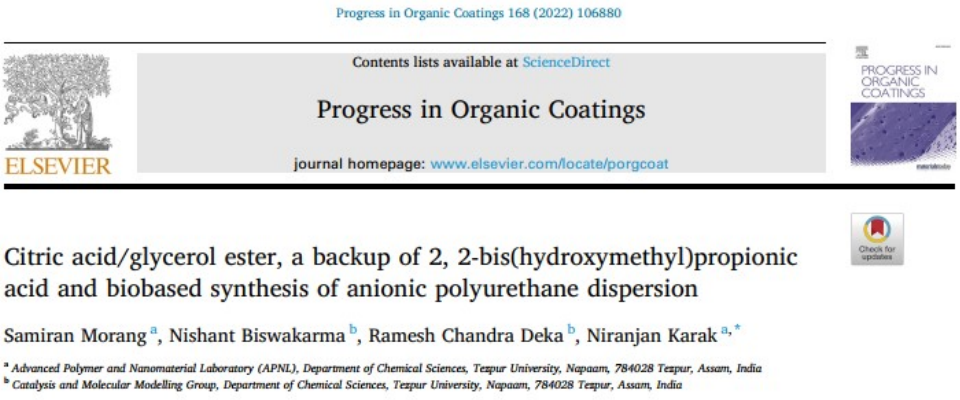

2.1. Introduction

Though quite old, polyurethane (PU) unzips new hope every year [1-2]. However, formulation and application of solvent-borne PUs are always associated with the liberation of an extensive amount of volatile organic compounds (VOCs) and hazardous air pollutants (HAPs) into the atmosphere, as discussed in **Chapter 1** [3]. Thus, waterborne PU (WPU) dispersions become an enthusiastic topic in PU chemistry and emerged as optimistic alternatives to their solvent-borne counterpart in terms of non-toxicity, non-flammability, and no or minimal VOC content [4-7]. Moreover, in recent years' environmental concerns, high crude oil prices, increasing shortages of fossil-fuel reserves, and so on have triggered a search to use bio-based raw materials for the production of WPU. Many articles and patents illustrated the synthesis and application of anionic PU dispersions (PUDs), prepared from vegetable oil-based polyols, diisocyanates (aliphatic and aromatic), and internal or external emulsifiers [8-12]. Internal emulsifiers are very popular because the particle sizes in the resulting PUDs are smaller, leading to better stability compared to external emulsifiers containing PUDs. 2,2-Bis(hydroxymethyl) propionic acid (DMPA) is widely used as an internal emulsifier for preparing anionic PUD. It functions as a chain extender in a polymerization reaction with diisocyanates, and its free carboxylic acid group in ionic form provides surface charge to PU particles, stabilizing PUDs in the water phase [13]. Although DMPA has been used for a long time for anionic PUD preparation, it is not derived from bio-renewable resources, and it has also some limitations that raised the demand for its replacement. First, DMPA has a relatively high melting temperature (185-190 °C) and it is homogenized with polyol relatively at high temperature (~ 140 °C). Subsequently, the mixture of DMPA and polyol needs to be cooled to 70-80 °C under continuous agitation to avoid precipitation of DMPA. In short, DMPA consumed a long time for the formation of the final product. Secondly, the prime-time requirement for film formation after casting is long [14] and lastly, the problem is caused by the incompatibility between the DMPA and soft segments in the PUD because of its small size [15].

So, the introduction of a new biobased polyol or chain extender with the prerequisite ionizable group would be the best alternative to DMPA. In this context, glycerol ester of citric (GECA) was prepared from glycerol and citric acid using *para*-toluenesulfonic acid (*p*-TSA) as the catalyst. Both DMPA and GECA contain one carboxylic group along and different numbers and types (primary, secondary, and tertiary) of hydroxyl groups. Finally, GECA was used as an internal emulsifier instead of DMPA for preparing anionic PUDs. Various properties including physico-chemical, thermo-mechanical, chemical resistance,

biodegradability, and UV-aging capabilities of PUDs were investigated. The properties of DMPA-based PUD were also compared with the newly synthesized PUD. The reactivity of GECA and DMPA with isophorone diisocyanate (IPDI) was evaluated using Density Functional Theory (DFT) calculations.

2.2. Experimental

2.2.1. Materials

IPDI (Sigma Aldrich, USA) is an odorless and colorless liquid at room temperature. It has molecular weight, density, and boiling point of 222.23 $gmol^{-1}$, 1.049 gmL^{-1}, and 158 °C, respectively.

Poly(ε-caprolactone) diol (PCL, Sigma Aldrich, USA) was used as the macroglycol with molecular weight, density, melting temperature, and a hydroxyl value of 2000 $gmol^{-1}$, 1.071 gmL^{-1}, 50 °C, and 54 $mgKOH\ g^{-1}$, respectively. PCL was dried in a vacuum at 70 °C for 12 h before use.

The citric acid (CA, PCL, Sigma Aldrich, USA) has molecular weight and a melting point of 192.124 $gmol^{-1}$ and 153-159 °C, respectively, and was dried in a vacuum at 70 °C for 12 h before use. It was used to prepare GECA.

Glycerol is a semi-viscous colorless liquid. It was purchased from Merck-India and its molecular weight and boiling point are 92.09 $gmol^{-1}$ and 290 °C, respectively. It was dried at 70 °C under vacuum for 6 h before use to prepare GECA.

DMPA (Sigma Aldrich, USA) is a DMPA is an odorless white crystalline solid used as an internal emulsifier. Molecular weight and melting points are 134.13 $gmol^{-1}$ and 190 °C, respectively, and dried at 70 °C under vacuum for 6 h prior to use.

Castor oil (Sigma Aldrich, USA), a colorless viscous liquid with a characteristic odor, was employed to prepare monoglyceride of castor oil (MG_{CO}) which serves as the biobased chain extenders. It has molecular weight and boiling point of 927 $gmol^{-1}$ and 313 °C, respectively, and was dried at 70 °C under vacuum for 6 h prior to use.

Calcium oxide (CaO, Merck, India) is an alkaline, caustic, crystalline solid with molecular weight, minimum assay, and a melting point of 56.07 $gmol^{-1}$, ≥97% and 2580 °C, respectively. This is used as the catalyst for preparing MG_{CO} from castor oil and glycerol.

Methanol (Merck, India) has a molecular weight, density, and boiling point of 32.04 $gmol^{-1}$, 0.792 gmL^{-1}, and 64.5 °C, respectively. It was used as a solvent in the solubility test.

Triethylamine (TEA, Sigma Aldrich, USA) was used as the neutralizing agent with a molecular weight of 101.19 $gmol^{-1}$ and a boiling point of 89.28 ℃.

Ethylenediamine (EDA, SRL, India) is a basic amine with an ammonia-like odor and was used as the chain extender. Molecular weight and boiling points are 101.19 $gmol^{-1}$ and 116 ℃, respectively.

p-TSA (Sigma Aldrich, USA) was used as the catalyst to catalyze the esterification reaction between glycerol and citric acid without further purification. It is a crystalline solid having molecular weight and melting point of 190.12 $gmol^{-1}$ and 103-106 ℃, respectively.

Xylene (Merck, India) is a colorless liquid and was double distilled before use to reduce viscosity in the PU reaction. Molecular weight, density, and boiling point are 106.16 $gmol^{-1}$, 0.864 gmL^{-1}, and 138.5 ℃, respectively.

N,N-Dimethylforamide (DMF, Merck, India) was also double distilled before use to solubilize GECA and DMPA. It is a colorless to pale yellow liquid with a fishy or ammonia-like odor. It has molecular weight, density, and boiling point of 73.09 $gmol^{-1}$, 0.948 gmL^{-1}, and 153 ℃, respectively.

Hydrochloric acid (HCl, diluted, Merck, India) has molecular weight and density of 36.5 $gmol^{-1}$ and 1.19 gmL^{-1}, respectively. The solution of HCl was used to evaluate the chemical resistance ability of PU films.

Sodium hydroxide (NaOH, Merck, India) has a molecular weight of 39.99 $gmol^{-1}$ and a melting point of 319 ℃. It was used to evaluate the chemical resistance ability of PUD films. The aqueous solution of NaOH was also used to evaluate the chemical resistance ability of PU films.

Sodium chloride (NaCl, Merck, India) with molecular weight and density of 58.44 $gmol^{-1}$ and 2.16 gmL^{-1}, respectively, and its solution was used in the chemical resistance test.

Ethanol (Merck, India) is a colorless and flammable liquid with a molecular weight of 46.07 $gmol^{-1}$, a density of 0.790-0.793 gmL^{-1}, a boiling point of 78.3 ℃, and a flash point of 12-16 ℃. The solution of ethanol was also employed in the chemical resistance test.

B. subtilis (BS, Gram-positive, MTCC 441) bacterial strains were employed for the biodegradation test. These are cultured and collected from Molecular Biology and Biotechnology (MBBT), Tezpur University, Assam-784028, India.

2.2.2. Method

2.2.2.1. General procedure for the synthesis of the monoglyceride of castor oil (MG_{CO})

MG_{CO} was prepared by glycerolysis of ester according to an earlier reported method [8]. Briefly, 4.6 g of castor oil (5 mM), 0.55 g of glycerol (6 mM), and 0.0023 g (0.055 wt% of castor oil) of CaO were taken in a three-neck round bottom flask equipped with a thermometer, a mechanical stirrer, and a nitrogen inlet. The reaction was performed at 225±2 ℃, and the solubility test (MG_{CO}: methanol = 1:3, v/v, room temperature) confirmed its completion.

2.2.2.2. General procedure for the synthesis of glycerol ester of citric acid (GECA)

GECA was synthesized by using an esterification reaction of citric acid and glycerol in the presence of p-TSA. Briefly, 2.4 g of citric acid (12.5 mM), 2.3 g of glycerol (25 mM), and 0.0012 g of p-TSA were taken in a three-neck round bottom flask in the same equipment and arrangement as mentioned above. The reaction was performed at 140±2 ℃ until the desired acid value was achieved. The acid value confirmed the completion of the reaction [16]. (Experimental value: 164.89 $mgKOHg^{-1}$and the theoretical value: 179.69 $mgKOHg^{-1}$).

2.2.2.3 General procedure for synthesizing polyurethane dispersions

Three PUDs were synthesized via the pre-polymerization technique. The reaction setup comprises a three-neck round bottom flask equipped with a mechanical stirrer, a nitrogen inlet, a thermometer pocket, and a Teflon septum. The formulations of all PUDs are presented in **Table 2.1**. In the first step, NCO terminated prepolymer was synthesized by the reaction between PCL (4 g, 2 mM) and IPDI (0.889 g, 4 mM) in 1 mL of xylene. The reaction was continued for 4-5 h at 70-80 ℃. The FTIR data analysis detected the free NCO groups. Then, the reaction temperature was lowered to 25-32 ℃, and 0.5 mL xylene was added to it to reduce the viscosity. In the second step, GECA was added and continued for 0.5 h. Successively, EDA (0.045 g, 0.75 mM) diluted in 1 mL THF, MG_{CO} (0.931 g, 2.5 mM), and the remaining amount of IPDI were added to the reaction chamber and the reaction was performed for 5 h at 70-120 ℃. To neutralize the free acidic groups of GECA, TEA (0.039 g, 0.39. mM) was added and stirred for 45 minutes at 300 rpm at 25-30 ℃. For preparing the aqueous dispersion, water was added to the reaction mixture with vigorous stirring (650 rpm) for 1 h at 25-30 ℃. Three different compositions, namely PUD-1, PUD-2, and PUD-3 were synthesized by varying the GECA content (**Table 2.1**). The used solvents were removed under reduced pressure at the end of the successful synthesis of each composition.

2.2.3. Computational study

Density functional theory (DFT) calculations have been performed using the Gaussian 09 to obtain the ground state structures, energies, and frequencies of the species of interest [17].

M06-2X functional along with 6-31+G(d,p) basis set was chosen to predict the accurate ground state structures for species containing C, H, N, and O atoms [18]. Recent studies have suggested that the M06-2X/6-31+G(d,p) combination is accurate in predicting ground state structures for such types of systems [19-21] Vibration frequency calculations are done to differentiate the stable intermediate species (IMs) from first-order saddle point or a transition state (TS). IMs have zero imaginary frequencies, while TS structure has one. The geometry optimization of a structure is carried out using the Berny algorithm and is confirmed with one imaginary frequency [22]. Intrinsic reaction coordinate (IRC) calculations are performed to check the fidelity of the reaction pathway where it links one TS with its two nearby IMs [23].

Table 2.1. Recipes for the synthesis of PUDs with a constant amount of ϵ-PCL (2 mM, 4 g).

Reactants/Compositions	**PUD-1**	**PUD-2**	**PUD-3**
ϵ-PCL (mM)	2	2	2
MG_{CO}(mM)	2.5	2.5	2.5
EDA (mM)	0.75	0.75	0.75
GECA (mM)	0	0.15	0.25
DMPA (mM)	0.4	0.15	0
IPDI (mM)	7.1	7.025	7
TEA (mM)	0.52	0.39	0.325
Hard segment (wt%)	39.47	39.47	39.56
Soft segment (wt%)	60.53	60.53	60.44
Biobased unit (wt%)	14.089	14.86	15.367
Branching unit (wt%)	0.008	0.011	0.013
NCO/OH	1	1	1
Solid content (%)	35	35	35

2.2.4. Characterization

2.2.4.1. Structural analysis

FTIR spectra of GECA and PUDs films were obtained by a Nicolet (Madison, USA) FTIR impact 410 spectrophotometer using KBR pellets in the frequency range 4000-400 cm^{-1}. A 400 MHz NMR spectrometer (JEOL, Japan) was used to elucidate the structure of GECA and PUDs using DMSO-d_6 and $CDCl_3$ as the solvents and TMS as the reference. The crystallinity of the films was examined using a D8 Focus XRD machine (Bruker AXS, Germany) with monochromatic Cu Kα radiation (1.540598 nm) over the range of 2θ= 10°-70°.

2.2.4.2. Measurement of physical properties

The molecular weight (number average molecular weight, Mn and weight average molecular weight, Mw) and polydispersity index (PDI) of the PUs were determined by Gel Permeation Chromatography using linear polystyrene as the standard (GPC, Waters, UK). The mini-gloss meter (Sheen Instrument Ltd., UK) measured the gloss values of the films. Furthermore, an automatic contact angle meter DropMaster (model- DMs-401, Kyowa Interface Science Co. Ltd., Japan) was used to measure the water contact angles of the films. A UV-visible spectrophotometer (Model No-EVOLUTION 300, Thermo Fisher, USA) with dual-matched silicon photodiodes (detector) performed the transparency test in the spectral range of 200-800 nm.

2.2.4.3. Measurement of mechanical properties

The stress-strain profiles for three different compositional PUD films were investigated as per the ASTM D 657 using a Universal Testing Machine (UTM model-WDW-10, JINAN, CHINA), with a 1.0 kN load cell and a 20 $mmmin^{-1}$ crosshead speed. Rectangular-shaped specimens of 50 × 10 mm^2 (length × width) were used for all three samples. An average value of at least three replicates of each sample was taken to obtain the correct values. The stress-strain curve provided tensile strength and percentage of strain at break. The toughness was determined accurately by integrating the area under the tensile stress-strain curve for each composition. The scratch hardness tester (model No-705, Sheen Instrument Ltd., UK) prevailed scratch hardness of the films with various weighing bars and a travel speed of 50 mm s^{-1}. The impact strength was determined as per the standard ASTM D1037 by falling weight method using an impact test having a maximum height of 1 m, manufactured by S.C. Dey & Co, Kolkata. Adhesive strength between wood-wood (W-W) and metal-metal (M-M) surfaces was evaluated by lap shearing test using the same UTM.

2.2.4.4. Measurement of thermal properties

The thermal stability of PUDs of different compositions was investigated by using a TGA-4000 (PerkinElmer, USA). All the samples were heated from 30 °C to 600 °C at a heating rate of 5 °Cmin^{-1}. The melting temperature (T_m) and glass transition temperature (T_g) were

determined from DSC 214 Polyma (NETZSCH, Germany). Here, all PUD films were heated at the same heating rate, i.e., 5 °Cmin^{-1} within a range of -50 °C to 120 °C. Both experiments run under pure nitrogen gas (N_2) as the purge gas at a flow rate of 30 mLmin^{-1} with a pressure of 2.3 bar.

2.2.4.5. Chemical resistance test

The chemical resistance of all the PUDs was evaluated by immersing small pieces of PUD film into different chemical media including acidic solution, basic solution, 10% NaCl solution, 20% ethanol solution, and tap water for 30 days. The weight loss percentages reflect the chemical resistance.

2.2.4.6. UV-aging test

PUDs films with the dimension of 5 cm × 1 cm (length × width) were used to study the artificial environmental effect on the mechanical properties. The UV-aging test was performed in a UV-light-containing chamber (Labtech, India) with a wavelength of irradiation and power of 256 nm and 8W, respectively for 135 h. The UV-resistance was calculated by the following equation:

$$\text{Retention, R}\ (\%) = 100 - \left[\frac{(P^0 - P^1)}{P^0}\right] \times 100 \qquad \textbf{Eq. 2. 1}$$

Where, P^0 and P^1 represent tensile strength before and after UV-aging, respectively.

2.2.4.7. Transparency test

A UV-visible spectrophotometer (Model No-EVOLUTION 300, Thermo Fisher, USA) with dual-matched silicon photodiodes (detector) performed the transparency test in the spectral range of 400-800 nm.

2.2.4.8. Biodegradation test

The bacterial degradation studies were performed by following the McFarland turbidity method using *B. subtilis* (a Gram-positive bacterial strain). A suitable environment was created by preparing a solution of 500 mL water and 12.5 g Luria Bertani Agar (HIMEDIA). The salt solution was sterilized inside an autoclave at 120 °C temperature and under a pressure of 103.5 kPa for 30 minutes. The bacterial strain was cultured in the prepared 10 mL salt solutions separately and incubated at 37 °C for 48 h with constant shaking. Subsequently, PUD films with rectangular geometry (1 × 2 cm^2) were sterilized by irradiating with the UV light of wavelength 254 nm. All the films were immersed in the bacterial solutions and incubated at 37 °C with constant shaking. The bacterial growth on the PUD

films was scrutinized by monitoring the weight loss and turbidity produced because of bacterial degradation. The absorbance was determined weekly by using a UV-spectrophotometer at 600 nm for up to five weeks. Finally, the surface morphology of all films was evaluated from SEM image analysis.

2.3. Results and discussion

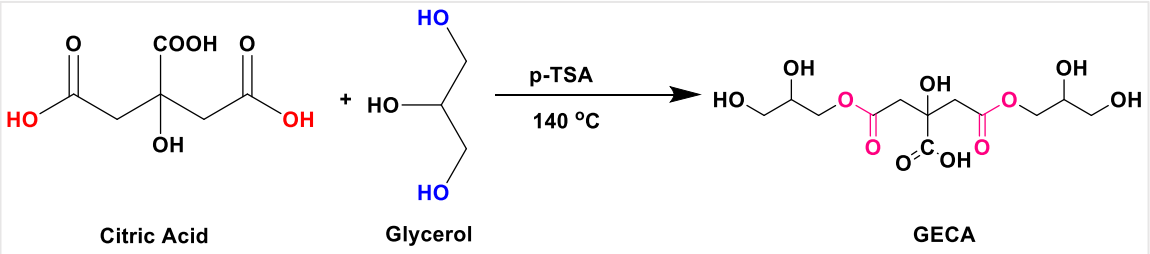

Scheme 2.1. Synthetic routes of GECA.

2.3.1. Synthesis and characterization of GECA

GECA was synthesized by the reaction between citric acid and glycerol in the presence of *p*-TSA at elevated temperature as shown in **Scheme 2.1**. Here it is pertinent to mention that GECA is not only the esterified product of citric acid and glycerol. But by considering the reactivity of hydroxyl and carboxylic groups of both the reactants and the mole ratio of them the representative structure of GECA as the major product is only considered here. The reactivity of the primary hydroxyl and carboxylic groups is much higher than the corresponding tertiary or even secondary groups, thus GECA is the most probable structure and for simplicity, it is only considered. GECA is soluble in highly polar solvents such as water, DMSO, NMP, and DMF, but less soluble or insoluble in less polar/nonpolar solvents such as THF, hexane, toluene, and xylene [24].

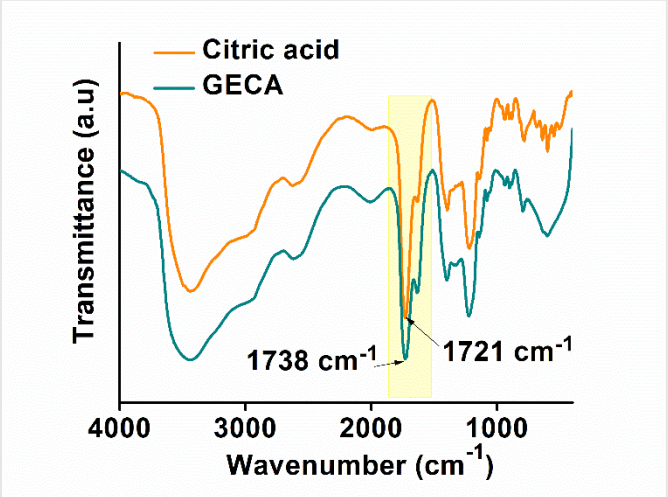

Figure 2.1. FTIR spectra of GECA and citric acid.

This is because of the free carboxylic acid group present in GECA, which was confirmed by FTIR analysis (**Figure 2.1**). The significant broad absorption peak at 3461 cm^{-1} corresponds to the hydroxyl group of carboxylic acid functionality of citric acid, but it was shifted slightly to 3449 cm^{-1} because of the increase in conjugation via esterification of terminal carboxylic acid groups.

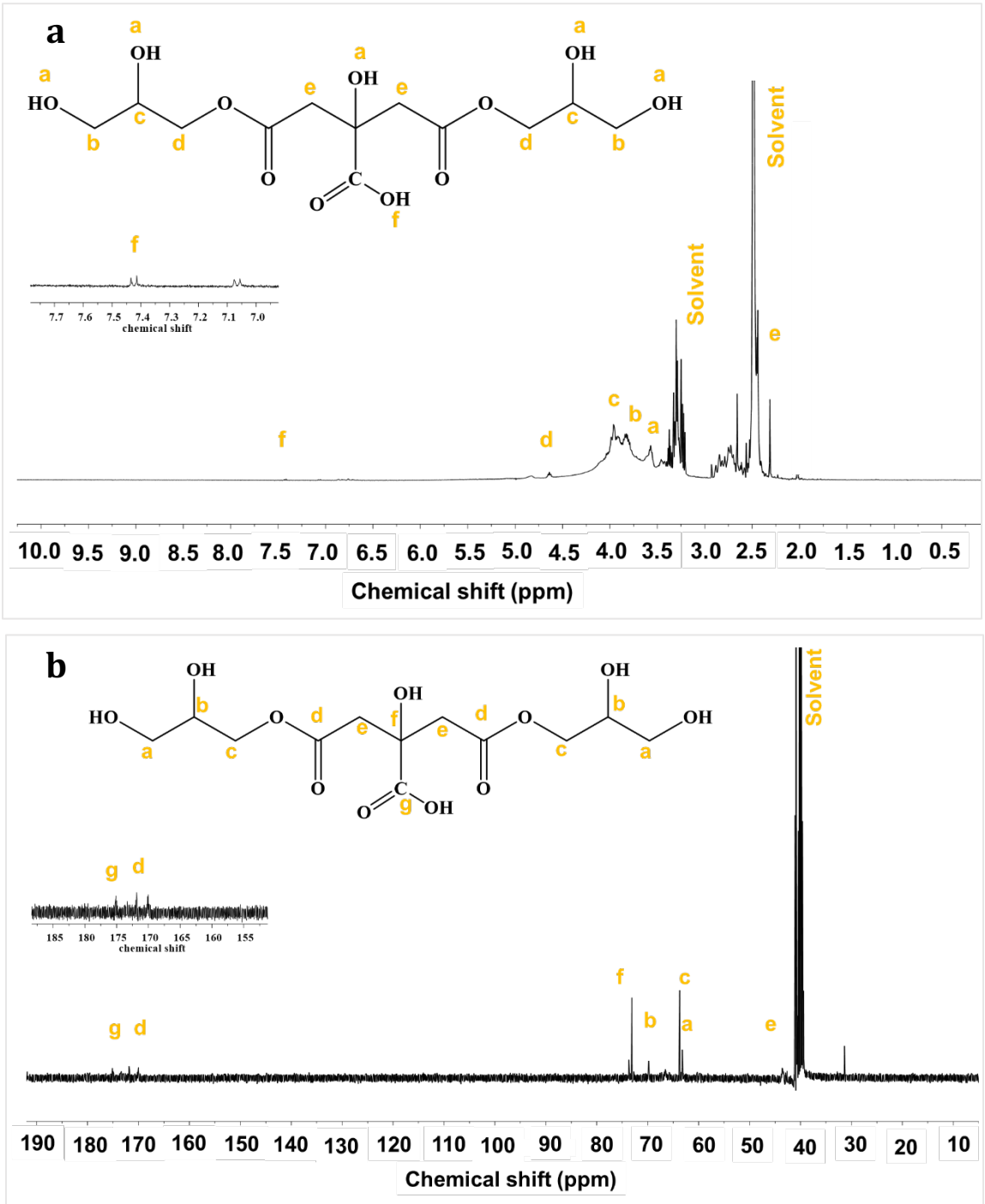

Figure 2.2. (a) ^{1}H NMR and (b) ^{13}C NMR spectra of GECA.

Two peaks for the citric acid moiety were observed at 1738 cm^{-1} and 1632 cm^{-1} assigned to free C=O and hydrogen-bonded C=O, respectively which were merged and shifted

slightly to 1721 cm^{-1} as seen in the FTIR spectra of GECA [25]. Again, the two small peaks at 1392 cm^{-1} and 943 cm^{-1} assigned were in-plane and out-of-plane vibrations of the O—H bond of carboxylic acid and found in only the citric acid spectrum, not in GECA. These peculiarities support the esterification of citric acid and glycerol. The chemical structure of GECA was characterized by ^{1}H and ^{13}C NMR spectroscopic studies. The peaks corresponding to proton and carbon atoms rising from different environments were interpreted as shown in **Figure 2.2 (a)** and **(b)**. In the ^{1}H NMR spectrum of GECA, the chemical shift value at 7.43 ppm (f) corresponds to the proton of the carboxylic group of the citric acid unit.

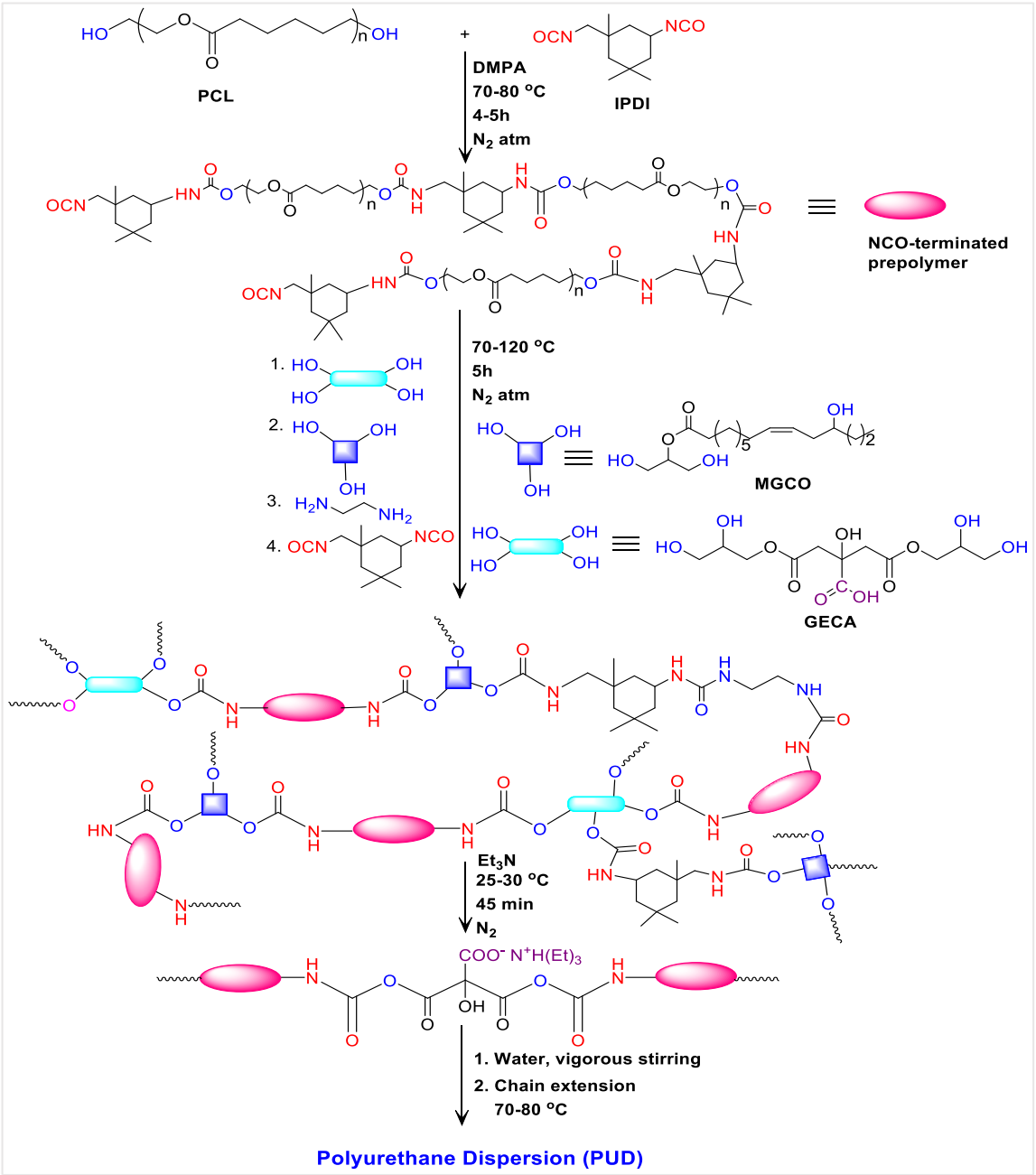

Scheme 2.2. General reaction pathway to synthesize PUD.

The peaks at 4.62 ppm (d), 3.96 ppm (c), and 3.56 ppm (a) can be assigned to α, β, and γ protons of the glycerol unit attached to the ester group. The peak at 2.31 ppm (e) corresponds to the methylene protons of the citric acid unit [26]. Concurrently, the ^{13}C spectrum of GECA was also evaluated and interpreted to ascribe different peaks. Peaks at 63.13 ppm (c), 69.67 ppm (b), and 63.66 ppm (a) can be attributed to α, β, and γ carbons of the glycerol unit associated with the ester group. The most downfield peaks at 171.65 ppm (d) and 175.14 ppm (g) correspond to the carbonyl carbon of the ester group and that of the carboxylic group, respectively [2]. The peak at 73.75 ppm (f) can be assigned to the tertiary carbon of the citric acid unit. Also, the peak at 42.1 ppm (e) shows methylene carbon of the same unit of GECA.

2.3.2. Synthesis and characterization of polyurethane dispersions (PUDs)

PUDs with three different compositions of GECA and DMPA were synthesized by the pre-polymerization technique, as shown in **Scheme 2.2**. FTIR spectral analysis validated the presence of a free NCO group in the prepolymer. The FTIR absorbance peaks of a prepolymer and all PUDs are shown in **Figure 2.3**. A simple inspection of the spectra reveals the characteristic peaks which support the successful synthesis of the desired product. Notably, the absence of the absorbance band at 2270-2250 cm^{-1} shows the zero availability of free NCO groups, which can be converted into either urethane or urea linkages in the PUDs [27].

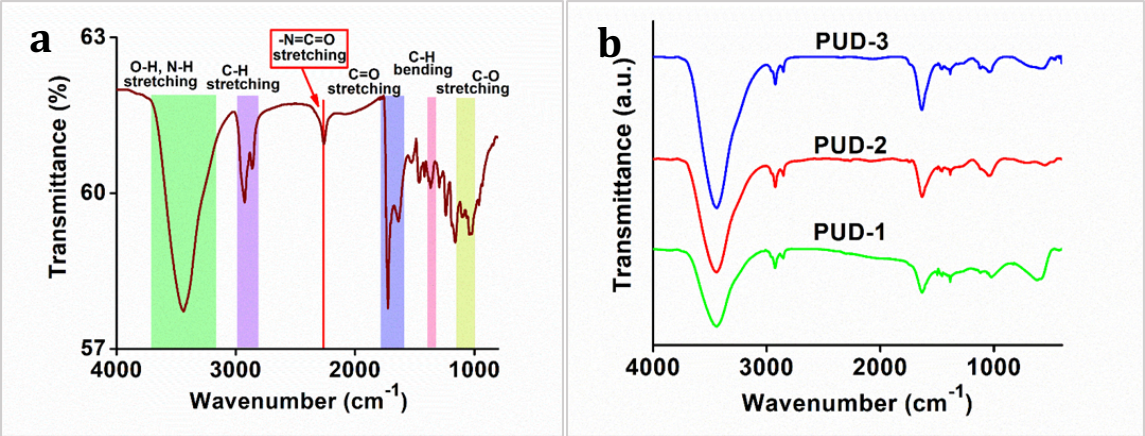

Figure 2.3. (a) FTIR spectrum of the prepolymer and (b) FTIR spectra of PUDs.

The broad band appeared near 3442 cm^{-1} attributed to the stretching vibrational frequency of hydrogen-bonded or free N—H group of the urethane bond and O—H group. The sharp band at 1737 cm^{-1} and the small weak band at 1639 cm^{-1} correspond to the C=O stretching vibration of the amide group of the urethane bond and that of the ester group, respectively. Again, the small weak band near 1470 cm^{-1} shows the N—H bending vibration. The band near 1129-1030 cm^{-1} can be ascribed to the stretching vibration of O—C=O and N—C groups. Thus, the IR data support the formation of urethane linkage (—O—CO—NH—) in the final product. The two distinct bands at 2920 cm^{-1} and 2853 cm^{-1} can be assigned to the asymmetric and

symmetric stretching of the sp^3 hybridized C—H bond. The small band near 1457-1380 cm^{-1} corresponds to the —CH_2 and —CH_3 bending vibrations. Finally, the proposed structure of the PUD was confirmed by ^1H and ^{13}C NMR spectral analyses. The ^1H NMR spectrum of the representative PUD-2 (containing both emulsifiers viz. GECA and DMPA) is shown in **Figure 2.4 (a)**. In the ^1H NMR spectrum, the three peaks at 0.89 ppm (a), 0.94 ppm (b), and 0.97 ppm (c) correspond to the methyl protons present in the IPDI and MG_{CO} moieties [28].

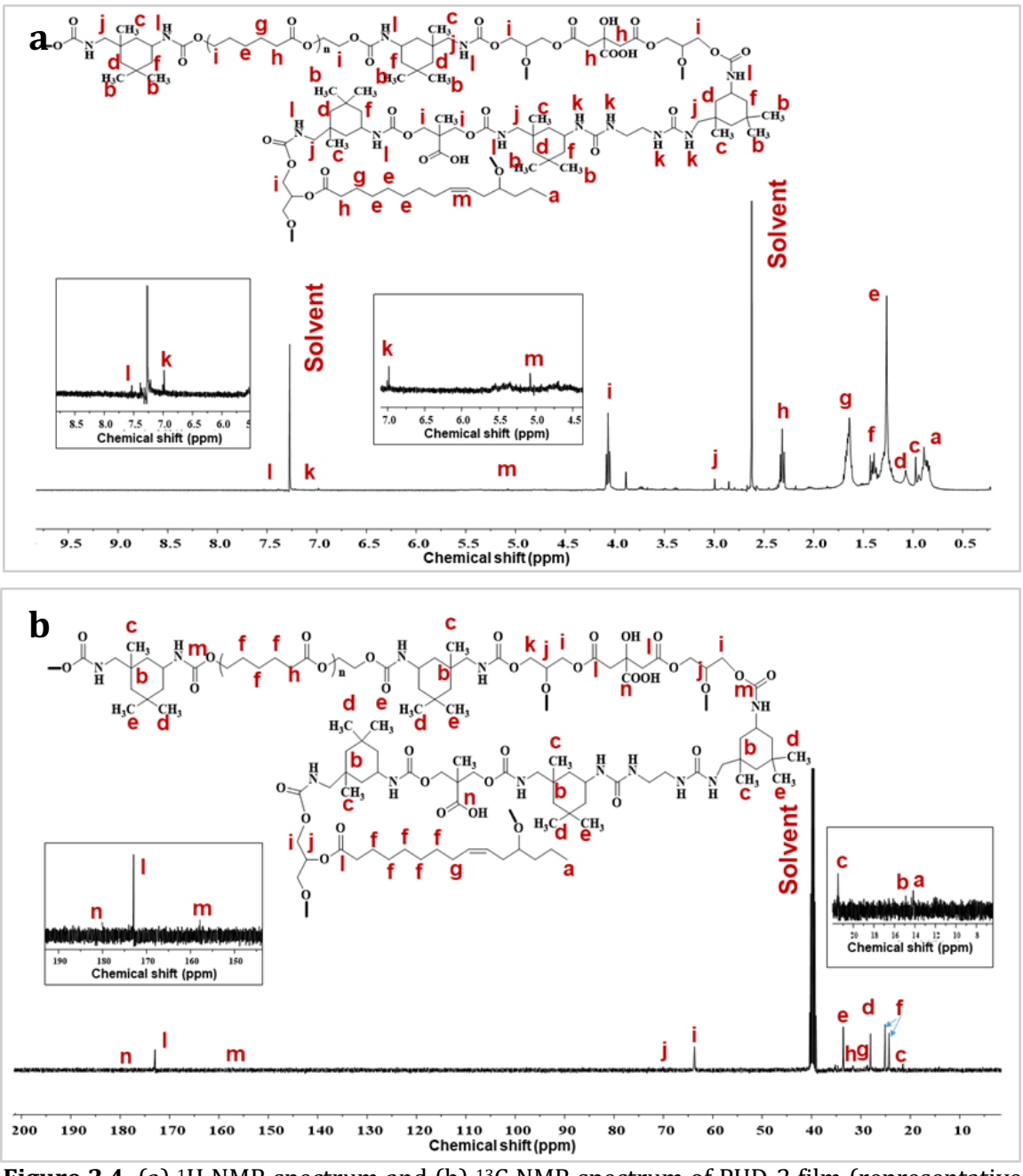

Figure 2.4. (a) ^1H NMR spectrum and (b) ^{13}C NMR spectrum of PUD-2 film (representative one).

The peak at 1.27 ppm (e) can be ascribed to the methylene protons of MG_{CO} and PCL units of PUD. Two peaks at 1.64 ppm (g) and 2.30 ppm (h) correspond to the protons attached with α and β carbons regarding the ester linkage. The peak at 4.07 ppm (i) can be assigned to the methylene proton attached to the carbon atom next to the oxygen atom of the urethane linkage. The MG_{CO} contains two methine groups and their corresponding chemical shift was found to be at 5.08 ppm (m). Peaks at 6.99 ppm (k) and 7.53 ppm (l) can be ascribed to the protons attached to the nitrogen atom of urea and urethane linkages, respectively. Thus, the data of the ^{1}H NMR spectrum support the expected chemical structure of PU. The ^{13}C NMR spectrum of the same composition is shown in **Figure 2.4 (b)**. Peaks at 21.53 ppm (c), 28.12 ppm (d), and 33.63 ppm (e) can be assigned to the three types of terminal methyl carbons present in the IPDI unit and the peak at 14.10 ppm (a) corresponds to the terminal methyl carbon of the MG_{CO} unit. The chemical shift for the methylene carbons of MG_{CO} and PCL moieties was found to be 24.93 ppm (f), 28.61 ppm (g), and 31.52 ppm (h). The peak at 63.70 ppm (i) can be ascribed to methylene carbon attached to the oxygen atom of urethane linkage [29]. On the most downfield side, the peak at 173.05 ppm (l) corresponds to the carbonyl carbon of the ester group of GECA and MG_{CO} moieties. Successively, two small peaks at 157.57 ppm (m) and 179.95 ppm (n) can be assigned to the carbonyl carbon of urethane linkage and free carboxylic group, respectively.

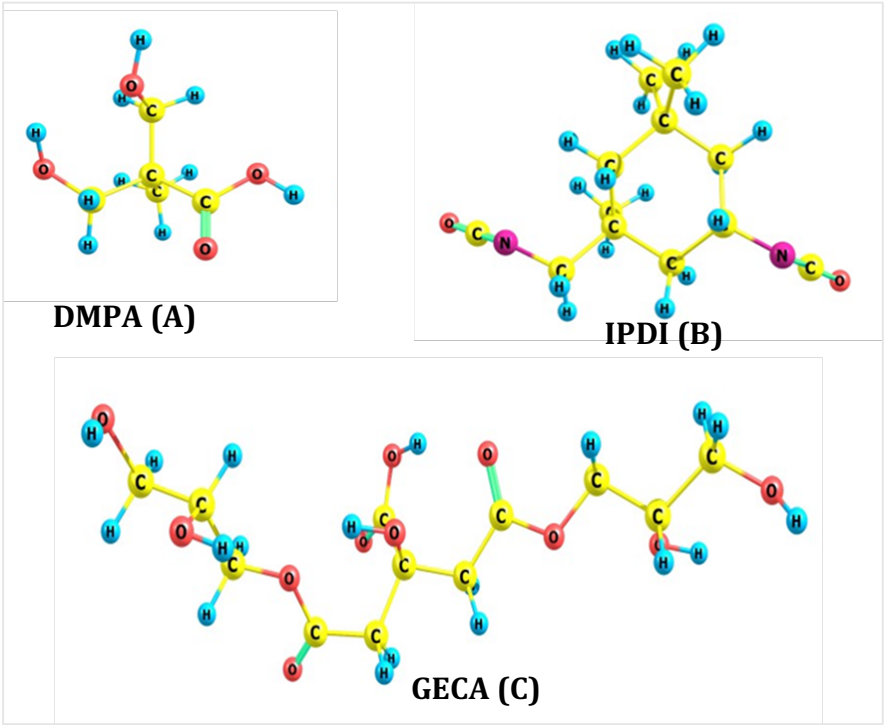

Figure 2.5. Optimized structures of DMPA (A), IPDI (B), and GECA (C).

2.3.3. Comparison of the reactivity of primary hydroxyl group present in DMPA and GECA with IPDI using DFT calculations

The optimized structures of DMPA, IPDI, and GECA are given in **Figure 2.5** and designated as A, B, and C, respectively. The DFT-based global descriptors were calculated using the energy of HOMO and LUMO which were derived by Koopmans's approximation [30]. Natural Bond Orbital (NBO) calculations were performed to find the HOMO-LUMO gap (HLG) through which the other descriptors can be derived. **Table 2.2** includes the DFT-based reactivity descriptors for DMPA, IPDI, and GECA. The species A and C must react with B to form a urethane bond, thus establishing intermediates (IM), IM1_A-B, and IM1_B-C as depicted in **Figure 2.6 (a)** and **(b),** respectively.

Table 2.2. The DFT-based reactivity descriptors (in eV) of DMPA (A), IPDI (B) and GECA (C).

Properties	**A**	**B**	**C**
HLG	9.442	9.114	9.320
Electronegativity	4.633	4.624	4.843
Hardness	4.721	4.557	4.660
Softness	0.105	0.109	0.107
Electrophilicity index	2.273	2.346	2.516

As shown in **Figure 2.6 (a)**, the relative Gibbs' free energies of all the species related to IM1_A-B at 298 K and 1 atmosphere were calculated. In IM1_A-B, it can be seen that DMPA (A) and IPDI (B) came closer to interacting with each other. The interaction energy of A-B is -6.224 kcal mol^{-1}. The reaction proceeds forward via TS1_A-B, where the primary —OH group of DMPA interacts with one of the —NCO groups of IPDI. The interaction is clear from the bond length of the —OH group of DMPA and the bond angle of N—C—O in IPDI. The bond length of the O—H group is 0.965 Å in IM1_A-B, whereas it increases to 1.157 Å in transition states (TS), TS1_A-B, thus showing its interaction with IPDI. Correspondingly, the N—C—O bond angle was 173° in IM1_A-B but interaction with the H atom of the —OH group changed it from linear to bent (145°). The H atom of the —OH group is going near the N atom of the —NCO group, which is obvious from the bond length of the N-H bond (1.383 Å) in TS1_A-B. Similarly, the O atom of the —OH group interacts with the C atom of the —NCO group to form the urethane bond. The TS is confirmed with one imaginary frequency of 1419.983 i cm^{-1}. Then, IM2_A-B is formed where H atom gets grouped and extra C—O bond is formed, thus creating a urethane bond. The activation energy of the reaction pathway is 32.213 kcal mol^{-1}. Overall, the reaction is exothermic with IM2_A-B lower in energy (-25.799 kcal mol^{-1}) regarding the starting point.

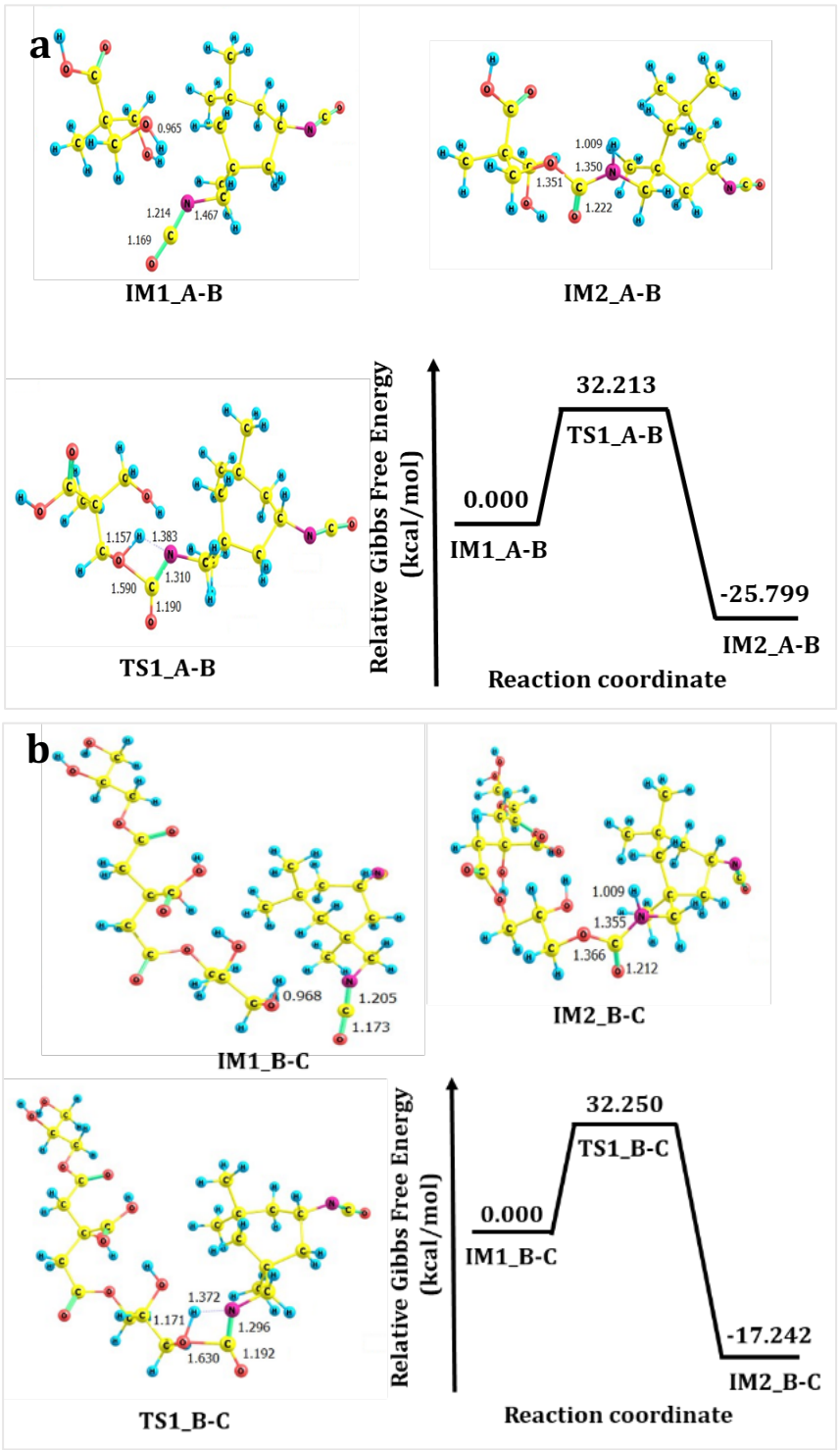

Figure 2.6. Optimized structures of intermediates (IM), transition states (TS), and potential energy diagram for (a) A–B and (b) B–C species interaction at M06-2X/6-31+G (d, p).

Similarly, relative Gibbs' free energies of all the species are calculated regarding IM1_B-C (**Figure 2.6 (b)**). TS interaction energy of IPDI with GECA (B-C) is found to be -12.028 kcalmol^{-1}. The reaction advances via TS1_B-C, where the H atom of the terminal ─OH group of GECA is getting transferred to the ─NCO group of IPDI. Elongation of the O─H bond

(0.968 Å to 1.171 Å) and formation of the N—H bond (1.372 Å) verifies the phenomenon. The bond angle of the —NCO group also changes from 173° in IM1_B-C to 147° in TS1_B-C. The formation of C—O bond (C atom of —NCO group and O atom of —OH group) can also be observed. The activation energy for the formation of a urethane bond with IPDI and GECA is 32.250 kcalmol^{-1}. TS is confirmed by its one imaginary frequency (1485.605 i cm^{-1}). Both the reaction pathways have comparable activation energy, and these are thermodynamically favorable. Thus, GECA can be used as a potential internal emulsifier for preparing DMPA free PUD.

2.3.5. Physical property of PUDs and its films

The values of all physical properties are presented in **Table 2.3**. The solubility test was performed with different solvents with an increasing order of polarity. The PUDs show good solubility in polar solvents such as THF, DMF, and DMSO, but low solubility or insolubility in non-polar solvents including hexane, xylene, etc. From this test, it can be confirmed that the PUD surface contains some polar functional groups like esters, carboxylic acids, and hydroxyl groups as well as urethane linkages along with the hydrocarbon backbone [2].

Table 2.3. Physical properties of PUDs and their films.

Property	PUD-1	PUD-2	PUD-3
Color (dispersion)	Milky white	Milky white	Milky white
Specific gravity	1.12	1.15	1.17
Gloss at 60^0	78.4±2	64.8±4	67.4±4
M_w (g/mol)	83665	62765	50919
M_n (g/mol)	55272	50042	36166
PDI	1.51	1.25	1.40

Specific gravities were determined by using a Pycnometer and the value varies between 1.12-1.17 which is closed to the previously reported data [16]. The average molecular weight of all PUDs was studied using GPC analysis, as demonstrated in **Figure 2.7 (a)** to **(c)**. The weight-average (M_w) and number-average molecular weights (M_n, gmol^{-1}) are 83665, 62765 and 50919, and 55272, 50042 and 36166 for PUD-1, PUD-2, and PUD-3, respectively. This gradual decrease in average molecular weight can be explained with the help of the degree of polymerization, which is the highest in PUD-1. The polydispersity index (PDI) values of PUD-1, PUD-2, and PUD-3 are 1.51, 1.25, and 1.40, respectively. Since the PDI values are low, so the polymeric chains are uniform up to a certain level which is supported

by the well-defined properties of all PUDs. Moreover, contact angles of PUD films in the range of 69° to 75° which refer to the hydrophilic nature, as shown in **Figure 2.7 (d)**. The XRD patterns at 2θ ranging from 10° to 70° of all three PUD films are presented in **Figure 2.7 (e).** According to an earlier report, the pure ε-PCL_{2000} (semi-crystalline) exhibited two main characteristic peaks at 2θ=21.4° and 23.8° corresponding to (110) and (200) reflection plans [31]. A broad peak between 2θ ~19.14°-20.54° was observed for all PUD films in the diffractograms. This can be attributed to the soft crystalline phase with the amorphous phase. Cross-linking of the polymer limits the chain entanglement and flexibility, resulting in low crystallinity.

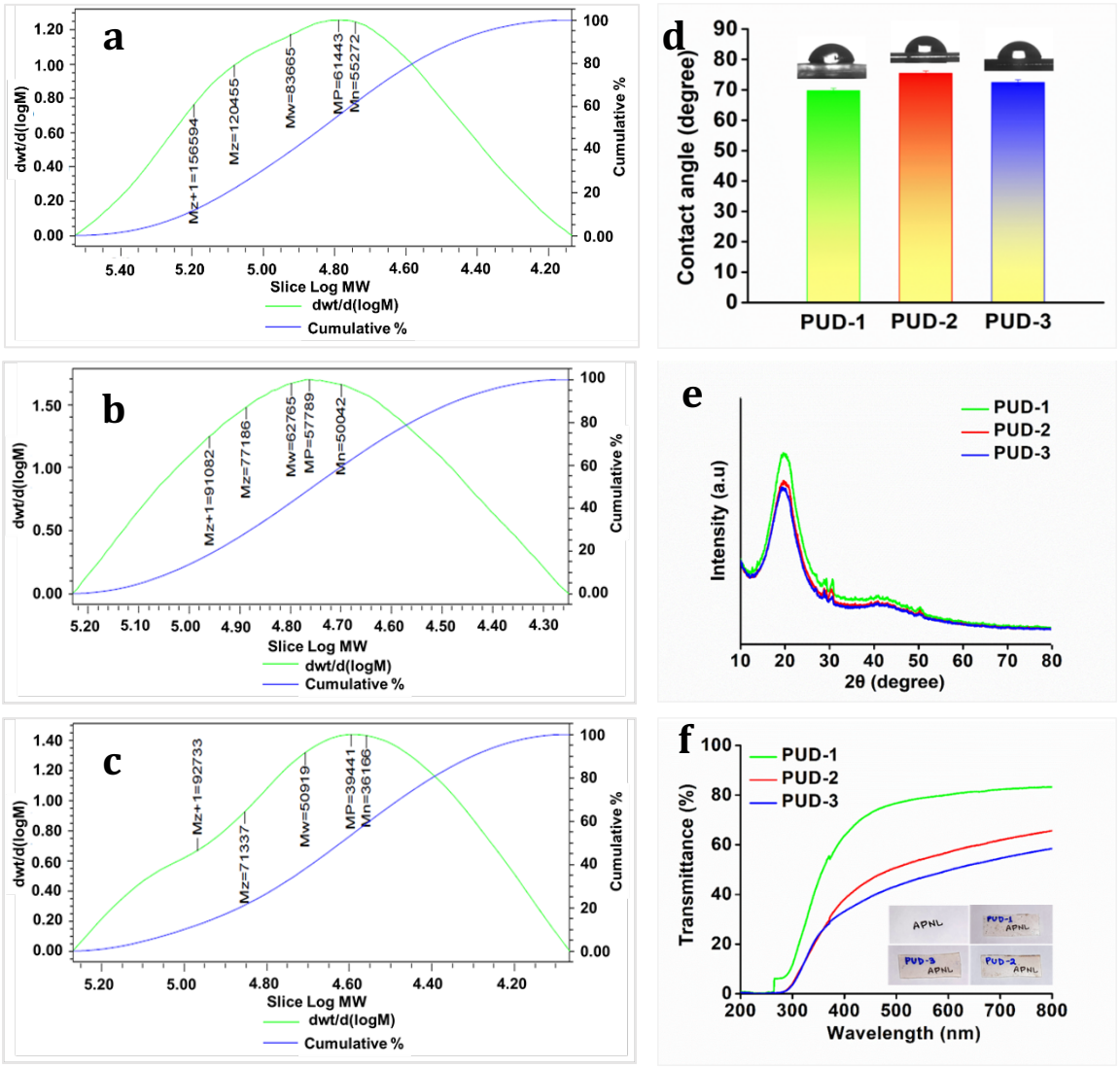

Figure 2.7. (a-c) GPC chromatograms of average molecular weight, (d)water contact angle, (e) P-XRD spectra, and (f) percentage of transmittance of PUD films.

Though the diffraction patterns of all three compositions were the same, the peak intensities decreased in the order of PUD-1 > PUD-2 > PUD-3 with increased GECA content. The GECA contains relatively more hydroxyl group which causes virtual cross-linking and

results in less crystallinity. Furthermore, the optical transparency was evaluated quantitatively for the films with thickness (t) of ~ 0.40 mm. All PUD films appeared colorless and transparent, and the word '**APNL**' under the film was visible clearly, as shown in **Figure 2.7 (f)**. The transmittance of the three compositions viz. PUD-1, PUD-2, and PUD-3 were 58.83%, 65.83%, and 83.31%, respectively. Literature reveals that the crystalline areas of a polymer are more densely packed than the amorphous areas. Also, high light scattering occurs on various boundaries between crystalline and amorphous regions of crystalline polymers, which makes them less transparent [32]. Furthermore, GECA is a transparent semi-liquid product that enhances the transparency of resultant PUD films. Thus, the higher the GECA percentage, the lower the crystallinity of PUD films. Thus, the percentage of transmittance increases with the increase in GECA content.

Table 2.4. Mechanical properties and adhesive strength of PUDs.

Property	PUD-1	PUD-2	PUD-3
Tensile strength (MPa)	10.58±0.41	7.00±0.39	6.39±0.37
Strain (%)	1656±117	1469±133	1833±121
Toughness (MJm^{-3})	95.71	65.47	71.27
Scratch hardness (kg)	9±2	7±2	4±1
Adhesive (W-W) (kPa)	13.06	18.96	43.29
Adhesive (M-M) (kPa)	0.814	0.56	0.14

2.3.6. Mechanical properties

The mechanical properties of all PUDs were evaluated and presented in **Table 2.4**. The quantitative values of these properties depend on many factors such as the average molecular weight of PUD, amount and composition of soft and hard segments, physical or virtual cross-linking, the entanglement of chains, orientation of segments, number of rigid moieties present, and non-covalent interactions e.g., hydrogen bonding, polar-polar interactions, and van der Waals forces. Tensile strength, strain (%) at break, and toughness are calculated from the corresponding stress-strain profiles, as shown in **Figure 2.8.** The stress-strain profiles show that all PUDs exhibited moderate tensile strength but high strain (%) at break. The high flexibility of the PUD arises mainly because of ε-PCL_{2000} moiety and long hydrocarbon chains in MG_{CO}. The greater value of chain entanglement can be achieved using segments with long hydrocarbon chains [33]. The optimized chemical structure

(**Figure 2.5**) obtained from theoretical studies shows that GECA has a longer hydrocarbon chain than that of DMPA.

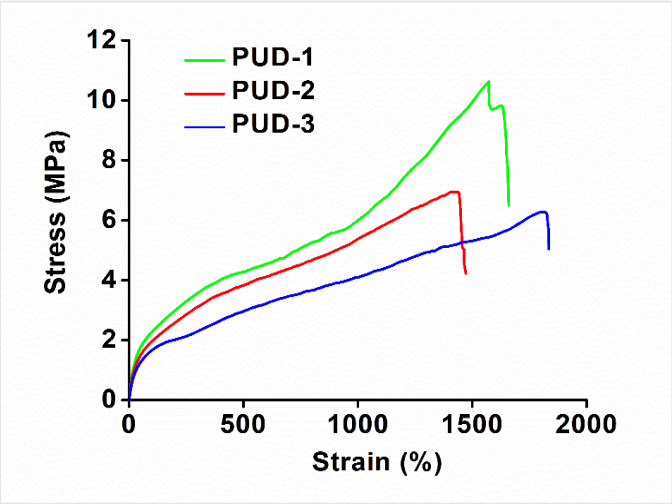

Figure 2.8. Stress–strain profiles of PUD films.

As expected, the highest elongation was found for the PUD-3, where GECA content is maximum. The toughness of the PUD films was calculated by integrating the area under the stress-strain curve for each composition. It is developed because of the chain entanglement, intermolecular interactions, and the crystallinity of the polymer matrix, chain extenders, and cyclic ring of IPDI. High strength and elongation resulted in high toughness. The impact resistance of all PUDs is satisfactory (greater than the maximum limit of the used instrument), and the reason seems to be the same, i.e., high strength and flexibility.

Table 2.5 Thermal properties of PUD films.

Parameter	PUD-1	PUD-2	PUD-3
T_1 (°C)	261.8	270.1	274.2
T_{MAX} (°C)	340.6	338.9	341.2
T_2 (°C)	423.5	431.7	438.4
T_g (°C) (hard segment)	51.2	55.5	67.5

The scratch hardness was evaluated to study the deformation of PUD films, which increases with the increase in the degree of polymerization. The adhesive properties of all PUDs for wood (W), W-W and metal (M), M-M surfaces were scrutinized using UTM. The adhesive strengths for PUD-1, PUD-2, and PUD-3 in the W-W surface were 13.06 kPa, 18.96

kPa, and 43.29 kPa, while in the M-M surface the values are 8.14 kPa, 0.56 kPa, and 0.14 kPa, respectively. The maximum adhesive strength was observed for PUD-3 adhesive for the W-W surface. The adhesive strength increases with the increase in the percentage of GECA. GECA has one free carboxylic acid group and one free hydroxyl group, which is not present in DMPA. Adhesive strength is related to the availability of polar groups in the polymer and on the surface. Therefore, the values are higher for W-W surfaces (polar) than that for M-M surfaces (non-polar) as presented in **Table 2.4.** Some non-covalent interactions are also raised on the wood surface, which resulted in high adhesive strength. The adhesive force between PUD and metal surface is developed from the mechanical interlocking due to the penetration of polymer segments in the void or pore of metal surfaces.

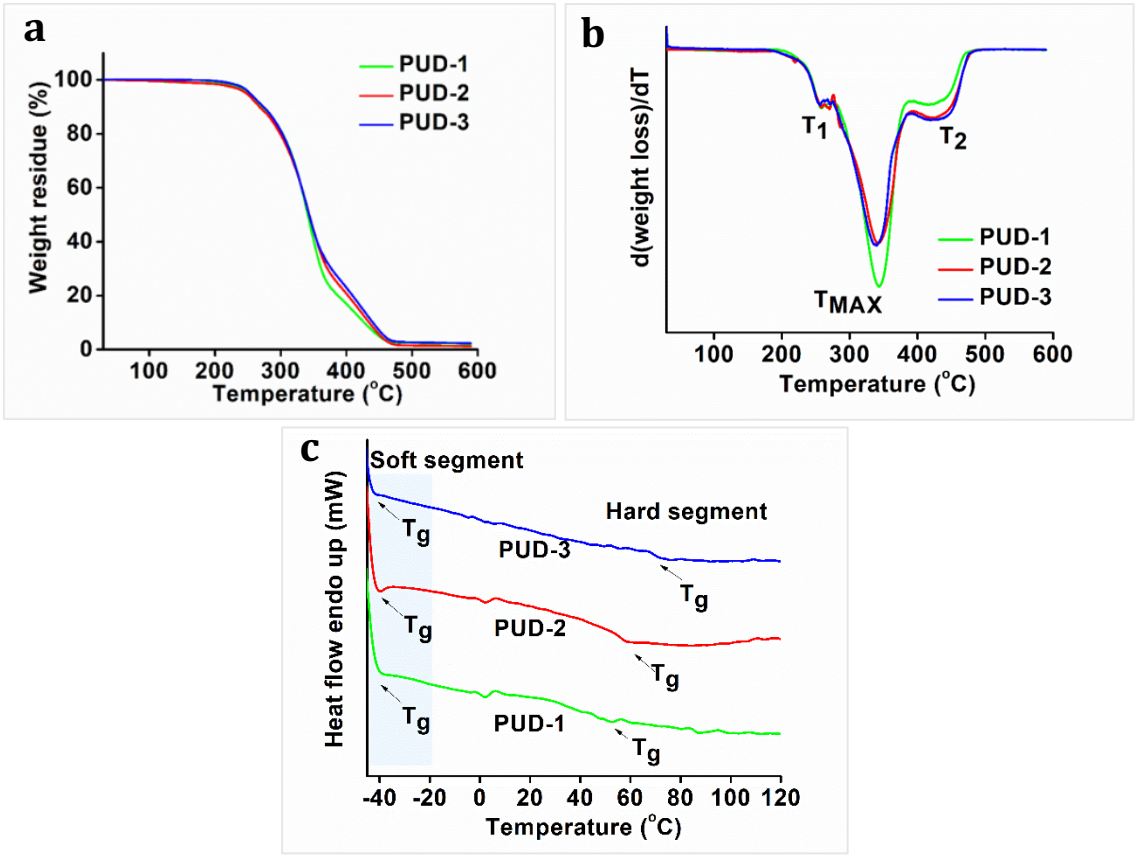

Figure 2.9. (a) TGA thermograms, (b) DTG curves, and (c) DSC curves of PUD films.

2.3.7. Thermal Properties

The TGA and DSC curves of the PUD films are shown in **Figure 2.9** and values are summarized in **Table 2.5.** The thermal stability of polyurethanes is low as the urethane linkages break down at a low temperature (300-350 °C). The factors responsible for thermal stability include the ratio of hard to soft segment of the matrix, the degree of polymerization, the molar mass and its distribution (PDI), and the extent of physical cross-linking. TGA and the first derivative of TGA (DTG) curves show the three steps of PUD degradation. The

maximum rate of mass loss (T_{max}) for PUD-1, PUD-2, and PUD-3 was found at 340.60 °C, 338.9 °C, and 341.2 °C, respectively. First-step degradation corresponds to thermo-labile moieties, for example, GECA and dehydration or elimination of entrapped water. Second-step degradation is related to more thermo-stable moieties, such as urethane, ester linkages, and MG_{CO}. The final step degradation is attributed to the degradation of the remaining segments (e.g., IPDI), the carbon char and ash formation processes. From **Table 2.5** and **Figure 2.9**, it can be confirmed that GECA plays an important role in the thermal stability of PUDs. Crosslinking density increases with GECA. Degradation temperature increases with the increase in the content of GECA, as seen from TGA and DTGA curves. The T_{ON}, T_{MAX}, and T_{END} increase with the increase in GECA percentage, and the maximum values were observed for PUD-3. As the GECA possesses two primary hydroxyl groups and two secondary hydroxyl groups, there will be more chances of urethane bond formation, leading to high physical cross-linking which results in high thermal stability of the final polymer [34]. Again, glass transition temperatures (T_g) of the soft segment and hard segment were measured from the DSC curves **(Figure 2.9 (c))**. The T_g of the soft segment was near -40 °C because of the ε-PCL_{2000} moieties. Again, the T_g of the hard segment was found between 51.2 °C to 67.5 °C. Thus, from the DSC curve, it can be concluded that the T_g of the hard segment increases with the increase in the amount of GECA and hence chemical cross-linking.

Table 2.6 Weight loss (%) of PUDs in different chemical media.

Chemical Medium	PUD-1	PUD-2	PUD-3
10% HCl	0.497	0.525	0.685
3% NaOH	3.116	4.138	4.532
10% NaCl	0.742	0.779	0.559
20% EtOH	0.222	0.207	0.154
Tap water	0	0	0

2.3.8. Chemical resistance study

The chemical resistance of PUDs films in five different chemical media including 10% hydrochloric acid (v/v, pH 4-5), 1% sodium hydroxide (w/v, pH 8-9), 10% NaCl (w/v), 20% ethanol (v/v) and tap water were scrutinized. The test was performed for one month and the values are close to earlier reported data [35]. From **Table 2.6**, it is noticed that all PUD films showed excellent chemical resistance in all the tested media except sodium hydroxide. This is because of strong non-covalent interactions, including H-bonding, van der Waal forces, and

high molecular weight. The low polydispersity index depicts the uniformity in the polymeric chain, which corresponds to fewer polymeric voids. Again, low resistivity towards alkali medium can be ascribed to the ester group present in PUD. The ester group easily undergoes base hydrolysis to form carboxylate salt and alcohol. The PUD-1 film (100% DMPA) shows relatively good resistance as it contains a lesser number of ester groups than that of other films.

2.3.9. UV-aging study

The exposure of polymeric materials to an aggressive environment such as UV radiation, thermal exposure and oxidative atmosphere causes significant changes in their physical, chemical and mechanical properties.

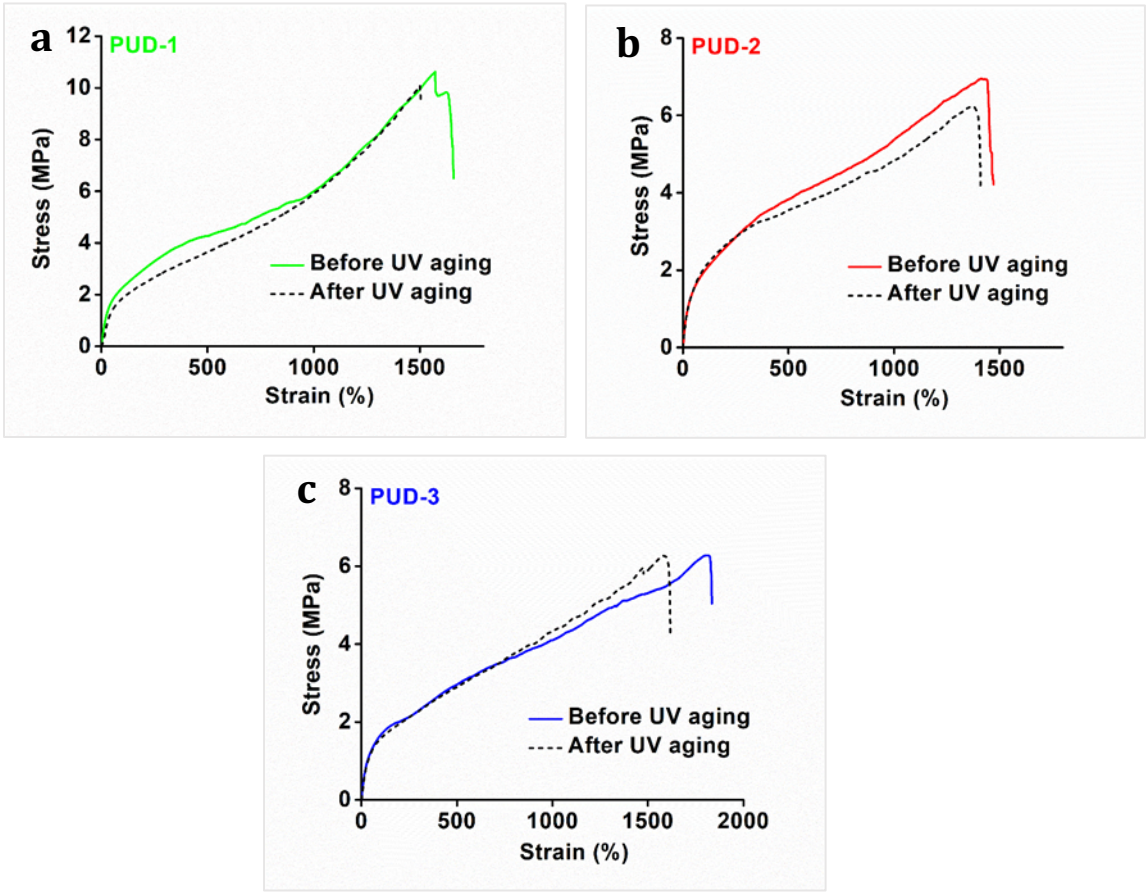

Figure 2.10. Stress-strain profiles of (a) PUD-1, (b) PUD-2, and (c) PUD-3, films after UV-aging for 135 h at 256 nm.

The natural testing weathering test is commonly used to evaluate the weather resistance property of the materials. But natural factors such as sunlight and weather variations (temperature and humidity) are difficult to control and time-consuming. Therefore, a UV-aging test was adopted to stimulate natural weathering conditions. To investigate the UV aging effect, changes in appearance and mechanical properties of PUDs films before and after UV exposure were examined. It was noticed that the color of the film changes from

transparent white to slightly light yellow. This change is attributed to the formation of an oxidized layer on the polyurethane surface [36]. **Figure 2.10** show a decrement in mechanical properties because of the UV light exposure. The changes in mechanical properties can be ascribed to the absorption of UV light by some moieties, for example, urea. PUD-3 possesses better UV resistance than other compositions because of the highest degree of branching and confined structure.

2.3.10. Biodegradation Study

The bacterial growth on the PUD films was studied with *B. subtilis* (Gram-positive strain). The biodegradation of the films was assessed by plotting optical density (OD) against the time of exposure, as shown in **Figure 2.11 (a)**. Also, the extent of biodegradation of PUDs was evaluated from SEM images taken after five weeks of exposure to bacterial strain. The SEM images and its 3D surface images shows that the bio-degraded films possess rougher surface than the control (un-degraded) films, as shown in **Figure 2.11 (b)** and **(c)**. Generally, the biodegradation process involves four steps namely, absorption of water, cleavage of ester linkages and undergoes hydrolysis to form oligomers such as carboxylic acid and diols, solubilization of these groups, and finally, transformation by bacteria to produce water, carbon dioxide, and humus [37]. Thus, biodegradation highly depends on the presence of hydrolysable ester and urea groups. The PUD-3 exhibits the highest bacterial growth because of the presence of many ester linkages in its structure. From the results, it is also clear that biodegradation increases with an increase in bio-based content from PUD-1 to PUD-3.

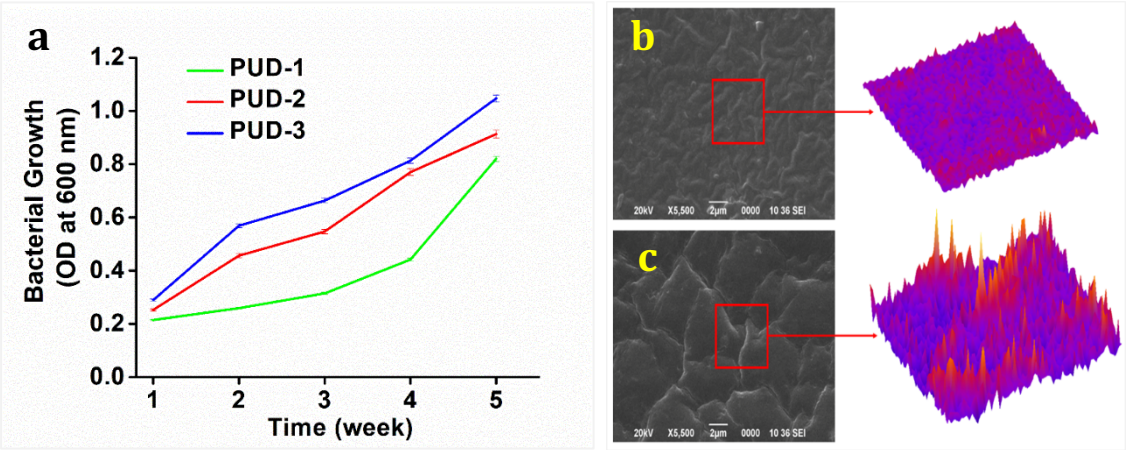

Figure 2.11. (a) Change in optical density (OD) of bacterial solutions at 600 with time and (b-c) SEM images of control (un-degraded) and degraded films and their respective 3D-surface plot obtained from ImageJ software.

2.4. Conclusion

In summary, a glycerol ester-based internal emulsifier (GECA) was used for preparing anionic polyurethane dispersions (PUDs). The reactivity of GECA is almost similar to

commercially used DMPA, as supported by DFT calculations. The FTIR, ^{1}H NMR, and ^{13}C NMR spectroscopic analyses confirmed the chemical structure of synthesized PUD. The results authenticated the favorable physicochemical attributes such as high tensile strength, outstanding flexibility, adhesive strength, good thermal stability, and transparency of the PUD films. Notably, all PUD films have the potential to resist different chemical media and UV radiation. Therefore, newly synthesized PUD can be used as an eco-friendly material for diverse applications, including surface coatings.

References

[1] Delebecq, E., Pascault, J. P., Boutevin, B. and Ganachaud, F. On the versatility of urethane/urea bonds: reversibility, blocked isocyanate, and non-isocyanate polyurethane. *Chemical Reviews*, 113(1):80-118, 2013.

[2] Karak, N. *Biobased Smart Polyurethane Nanocomposites: From Synthesis to Applications*. Royal Society of Chemistry, London, 2017.

[3] Zhang, C., Liang, H., Liang, D., Lin, Z., Chen, Q., Feng, P. and Wang, Q. Renewable castor-oil-based waterborne polyurethane networks: simultaneously showing high strength, self-healing, processability and tunable multishape memory. *Angewandte Chemie International Edition*, 60(8):4289-4299, 2021.

[4] Visser, S. A. and Cooper, S. L. Comparison of the physical properties of carboxylated and sulfonated model polyurethane ionomers. *Macromolecules*, 24(9):2576-2583, 1991.

[5] Narayan, R., Chattopadhyay, D. K., Sreedhar, B., Raju, K. V. S. N., Mallikarjuna, N. N. and Aminabhavi, T. M. Synthesis and characterization of crosslinked polyurethane dispersions based on hydroxylated polyesters. *Journal of Applied Polymer Science*, 99(1):368-380, 2006.

[6] Eisenberg, A. Clustering of ions in organic polymers. A theoretical approach. *Macromolecules*, 3(2):147-154, 1970.

[7] Dieterich, D., Keberle, W. and Witt, H. Polyurethane ionomers, a new class of block polymers. *Angewandte Chemie International Edition in English*, 9(1):40-50, 1970.

[8] Kalita, H. and Karak, N. Biobased hyperbranched shape-memory polyurethanes: effect of different vegetable oils. *Journal of Applied Polymer Science*, 131(1):1-8, 2014.

[9] Madbouly, S. A., Xia, Y. and Kessler, M. R. Rheological behavior of environmentally friendly castor oil-based waterborne polyurethane dispersions. *Macromolecules*, 46(11):4606-4616, 2013.

[10] Saalah, S., Abdullah, L. C., Aung, M. M., Salleh, M. Z., Biak, D. R. A., Basri, M. and Jusoh, E. R. Waterborne polyurethane dispersions synthesized from jatropha oil. *Industrial Crops and Products*, 64:194-200, 2015.

[11] Gurunathan, T., Mohanty, S. and Nayak, S. K. Effect of reactive organoclay on physicochemical properties of vegetable oil-based waterborne polyurethane nanocomposites. *RSC Advances*, 5(15):11524-11533, 2015.

[12] Lu, Y. and Larock, R.C. New hybrid latexes from a soybean oil-based waterborne polyurethane and acrylics via emulsion polymerization. *Biomacromolecules*, 8(10)3108-3114, 2007.

[13] Xia, Y. and Larock, R. C. Castor-oil-based waterborne polyurethane dispersions cured with an aziridine-based crosslinker. *Macromolecular Materials and Engineering*, 296(8):703-709, 2011.

[14] Kim, B., Yang, J., Yoo, S. and Lee, J. Waterborne polyurethanes containing ionic groups in soft segments. *Colloid and Polymer Science*, 281:461-468, 2003.

[15] Yang, C. Z., Grasel, T. G., Bell, J. L., Register, R. A. and Cooper, S. L. Carboxylate-containing chain-extended polyurethanes. *Journal of Polymer Science Part B: Polymer Physics*, 29(5):581-588, 1991.

[16] Chandra, S. and Karak, N. Environmentally friendly polyurethane dispersion derived from dimer acid and citric acid. *ACS Sustainable Chemistry & Engineering*, 6(12):16412-16423, 2018.

[17] Frisch, M. J., Trucks, G. W., Schlegel, H. B., Scuseria, G. E., Robb, M. A., Cheeseman, J. R., Scalmani, G., Barone, V., Mennucci, B., Petersson, G. and Nakatsuji, H. Gaussian 09, Revision D. 01, Gaussian, Inc., Wallingford CT. *See also: URL: http://www. gaussian. com*., 2009.

[18] Zhao, Y. and Truhlar, D. G. The M06 suite of density functionals for main group thermochemistry, thermochemical kinetics, noncovalent interactions, excited states, and transition elements: two new functionals and systematic testing of four M06-class functionals and 12 other functionals. *Theoretical chemistry accounts*, 120:215-241, 2008.

[19] Srinivasulu, G. and Rajakumar, B. Theoretical investigations on the kinetics of H-abstraction Reactions from CF3CH (OH) CF3 by OH radicals. *The Journal of Physical Chemistry A*, 117(22):4534-4544, 2013.

[20] Gour, N. K., Mishra, B. K., Hussain, I. and Deka, R. C. Theoretical investigation on the kinetics and thermochemisty of H-atom abstraction reactions of 2-chloroethyl methyl ether (CH 3 OCH 2 CH 2 Cl) with OH radical at 298 K. *Structural Chemistry*, 27:1491-1499, 2016.

[21] Paul, S., Gour, N. K. and Deka, R. C. Mechanistic investigation of the atmospheric oxidation of bis (2-chloroethyl) ether (ClCH 2 CH 2 OCH 2 CH 2 Cl) by OH and NO 3 radicals and Cl atoms: a DFT approach. *Journal of Molecular Modeling*, 25:1-9, 2019.

[22] Schlegel, H. B. Optimization of equilibrium geometries and transition structures. *Journal of Computational Chemistry*, 3(2):214-218, 1982.

[23] Gonzalez, C. and Schlegel, H. B. Improved algorithms for reaction path following: higher-order implicit algorithms. *The Journal of Chemical Physics*, 95(8):5853-5860, 1991.

[24] Xiao, Y., Fu, X., Zhang, Y., Liu, Z., Jiang, L. and Lei, J. Preparation of waterborne polyurethanes based on the organic solvent-free process. *Green Chemistry*, 18(2):412-416, 2016.

[25] Jiugao, Y., Ning, W. and Xiaofei, M. The effects of citric acid on the properties of thermoplastic starch plasticized by glycerol. *Starch-Stärke*, 57(10):494-504, 2005.

[26] del Campo, G., Berregi, I., Caracena, R. and Santos, J.I. Quantitative analysis of malic and citric acids in fruit juices using proton nuclear magnetic resonance spectroscopy. *Analytica Chimica Acta*, 556(2):462-468, 2006.

[27] Zhang, C., Wang, H., Zeng, W. and Zhou, Q. High biobased carbon content polyurethane dispersions synthesized from fatty acid-based isocyanate. *Industrial & Engineering Chemistry Research*, 58(13), pp.5195-5201, 2019.

[28] Prabhakar, A., Chattopadhyay, D. K., Jagadeesh, B. and Raju, K. V. S. N. Structural investigations of polypropylene glycol (PPG) and isophorone diisocyanate (IPDI)-based polyurethane prepolymer by 1D and 2D NMR spectroscopy. *Journal of Polymer Science Part A: Polymer Chemistry*, 43(6):1196-1209, 2005.

[29] Gorna, K., Polowinski, S. and Gogolewski, S. Synthesis and characterization of biodegradable poly (ϵ-caprolactone urethane)s. I. Effect of the polyol molecular weight, catalyst, and chain extender on the molecular and physical characteristics. *Journal of Polymer Science Part A: Polymer Chemistry*, 40(1):156-170, 2002.

[30] Foster, A. J. and Weinhold, F. Natural hybrid orbitals. *Journal of the American Chemical Society*, 102(24):7211-7218, 1980.

[31] Trovati, G., Sanches, E. A., Neto, S. C., Mascarenhas, Y. P. and Chierice, G. O. Characterization of polyurethane resins by FTIR, TGA, and XRD. *Journal of Applied Polymer Science*, 115(1):263-268, 2010.

[32] Ma, Z., Hong, Y., Nelson, D. M., Pichamuthu, J. E., Leeson, C. E. and Wagner, W. R. Biodegradable polyurethane ureas with variable polyester or polycarbonate soft

segments: Effects of crystallinity, molecular weight, and composition on mechanical properties. *Biomacromolecules*, 12(9), 3265-3274, 2011.

[33] Hojabri, L., Kong, X. and Narine, S. S. Novel long chain unsaturated diisocyanate from fatty acid: synthesis, characterization, and application in bio-based polyurethane. *Journal of Polymer Science Part A: Polymer Chemistry*, 48(15):3302-3310, 2010.

[34] Ni, B., Yang, L., Wang, C., Wang, L. and Finlow, D. Synthesis and thermal properties of soybean oil-based waterborne polyurethane coatings. *Journal of Thermal Analysis and Calorimetry*, 100(1):239-246, 2010.

[35] Deka, H. and Karak, N. Bio-based hyperbranched polyurethanes for surface coating applications. *Progress in Organic Coatings*, 66(3):192-198, 2009.

[36] Boubakri, A., Guermazi, N., Elleuch, K. and Ayedi, H. F. Study of UV-aging of thermoplastic polyurethane material. *Materials Science and Engineering: A*, 527(7-8):1649-1654, 2010.

[37] Rydz, J., Sikorska, W., Kyulavska, M. and Christova, D. Polyester-based (bio) degradable polymers as environmentally friendly materials for sustainable development. *International Journal of Molecular Sciences*, 16(1):564-596, 2014.